PAPER

Preparation of hyper-cross-linked hydroxylated polystyrene for adsorptive removal of methylene blue†

Fada Li, Jun Liu, Wenxiu Liu, Yuanyuan Xu, Yiwen Cao, Bo Chen [ID] and Mancai Xu [ID] *

A series of hydroxylated polystyrene (PS-OH) resins were prepared from macroporous poly(styrene-*co*-divinylbenzene) by nitration, reductive amination, diazotation and hydrolysis in sequence, and then a series of hyper-cross-linked hydroxylated polystyrene (HCPS-OH) resins were successfully prepared from the PS-OH resins by the Friedel–Crafts post-cross-linking using dichloromethane as an external cross-linker. Benefiting from the synthetic protocol, the HCPS-OH resins showed better adsorption performance for methylene blue in aqueous solution as compared with the corresponding PS-OH resins. HCPS-OH-4, one of the fabricated HCPS-OH resins which had the hydroxyl content of 5.0 mmol g^{-1} and BET specific surface area of 69.0 m^2 g^{-1}, showed the highest adsorption capacity and selectivity for methylene blue. Higher temperature, higher pH, and higher ionic strength were beneficial to adsorption of methylene blue from aqueous solution. HCPS-OH-4 could be regenerated by treatment with 1.0 M HCl methanol solution and deionized water sequentially. Moreover, HCPS-OH-4 retained good adsorption performance for methylene blue even after 5 cycles of adsorption and regeneration, which implied that it was a good candidate for adsorptive removal of methylene blue dye in waste water.

1. Introduction

Methylene blue (MB) is heavily used in printing and dyeing as a synthetic dye because of its good color stability and water solubility. However, MB existing in waste water might cause environmental impacts and human health risks such as megrim, nausea and jaundice due to its chemical stability and physiological toxicity. Therefore, MB needs to be removed from waste water before discharge. Many methods, including membrane filtration,[1–3] bio-degradation,[4–6] electro-catalytic or photo-catalytic degradation,[7–11] and liquid–liquid extraction,[12] are applied to remove MB from water, but the high operation cost of these methods limits their application in practice, especially at a large scale. Adsorptive separation is a competitive technology for removal of dyes from waste water, and several adsorbents such as mesoporous silica,[13] clay,[14,15] modified graphene,[11,16] biomass[17,18] and activated carbon[19–21] have been reported to remove MB from water. Overall, mechanisms of the adsorbents adsorbing MB from aqueous solution include physical adsorption, π–π interactions, hydrogen bonding, electrostatic interaction and ion exchange,[13,20] and thus materials with appropriate pore size distribution, high surface area,

a hydrophobic matrix and polar functional groups would be efficient adsorbents for removal of MB from water.

Polar-modified porous materials (PPMs), as materials with an appropriate pore size distribution, high surface area and diverse functionality, are reported to find use in several fields including waste water treatment,[22–24] separation,[25] catalysis,[26] gas capture and storage,[27–29] and so on. As a type of PPM with excellent adsorption performance, polar-modified hyper-cross-linked polystyrene (PHPS) resins are widely used in adsorptive removal of organic pollutants from aqueous solution due to their adjustable porosity, high specific surface area and hydrophilicity.[30–35] There are three strategies for preparation of PHPS. The first is to prepare polar initial styrene (St) co-polymers before post-cross-linking by adding polar monomers such as triallyl isocyanurate, methyl methacrylate, and *N*-vinyl-iminazole.[36–39] The second is to functionalize the hyper-cross-linked polystyrene (HCPS) through the reaction of chloromethyl groups with polar aromatics or amines during or after the Friedel–Crafts post-cross-linking of chloromethylated polystyrene (CMPS).[32,40] The third is to introduce phenolic hydroxyl groups through reaction of CMPS with phenols before post-cross-linking with formaldehyde dimethyl acetal (FDA).[33,41] However, these strategies for preparing the PHPS resins have to use expensive cross-linkers or carcinogenic reagent chloromethyl methyl ether (CMME). Meanwhile, introduction of polar groups limits the post-cross-linking degree which might lower the specific surface area of the PHPS resins.

College of Chemistry and Chemical Engineering, Hunan Normal University, Changsha, 410081, China. E-mail: romann@hunnu.edu.cn

The work of Sellaoui and co-workers revealed that the hydroxyl groups of biomass surface were the main responsible functional groups for MB adsorption.[18] If PHPS resins abundant with hydrogen and oxygen functionalities were used as the adsorbents for MB removal, MB would be removed from water efficiently, and thus we designed and prepared a series of hydroxyl enriched PHPS resins for MB removal, which were the hyper-cross-linked hydroxylated polystyrene (HCPS-OH) resins. In this work, a series of hydroxylated polystyrene (PS-OH) resins with different content of hydroxyl groups were prepared from poly(styrene-co-divinylnenzene) (PS-co-DVB) by nitration, reductive amination, diazotation and hydrolysis sequentially, and then the PS-OH resins were post-cross-linked through the Friedel–Crafts reaction with dichloromethane (DCM) to obtain a series of HCPS-OH resins, and adsorption performance of the resins for MB in aqueous solution was investigated.

2. Experimental

2.1. Materials

Macroporous PS-co-DVB resin was supplied by Jinkai Resin Chemical Co., Ltd (Jiangsu, China), it had cross-linking degree of 6%, total pore volume (V_{total}) of 0.039 cm^3 g^{-1}, average pore size (D_P) of 24.3 nm and BET surface area (S_{BET}) of 19.5 m^2 g^{-1}. Anhydrous FeCl$_3$, nitric acid, sulfuric acid, hydrochloric acid, acetic anhydride, sodium sulfite, 1,2-dichloroethane (DCE), DCM, aniline (AN) and p-nitroaniline (PNA) were obtained from Sinopharm Chemical Reagent Co., Ltd. SnCl$_2$·6H$_2$O was supplied from Xilong Scientific Co., Ltd (Shantou, China). Methylene blue (MB) was purchased from Macklin Biochemical Co., Ltd (Shanghai, China).

2.2. Preparation of HCPS-OH

In Scheme 1, 20 g PS-co-DVB resin and 100 g DCE was added and swelled at room temperature for 6 h, and then DCE was siphoned. Acetic anhydride was added, and stirred for 1 h. Nitric acid was added dropwise with the flask cooled in ice-water bath, and then the nitration reaction was proceeded by changing the reaction time and temperature to prepare a series of nitrated polystyrene (PS-NO$_2$) resins with various nitration degree. Subsequently, the PS-NO$_2$ resins were reductively aminated, diazotated and hydrolyzed sequentially to prepare a series of PS-OH resins according to the procedure described in ref. 42. The PS-OH resins were swollen in 150 mL DCM in

a three-necked flask overnight at room temperature, and then 30 g anhydrous FeCl$_3$ was charged to catalyze the Friedel–Crafts reaction between the phenyl of PS-OH and DCM. The reaction mixtures were heated for 24 h at 40 °C under stirring. The liquid phase was siphoned, and the solid samples were washed with ethanol for three times, extracted with ethanol in a Soxhlet extractor for 24 h, washed with 1.0 M NaOH and 1.0 M HCl respectively, then washed with deionized water to neutral, and thus the HCPS-OH resins were obtained. Further details of the reaction conditions were displayed in Tables S1–S3.†

2.3. Characterization

Functional groups of the resins were characterized via the Fourier transform infrared spectrometer (Avatar 370, USA). The X-ray photoelectron spectroscopy (XPS) of the resins was carried out using the Thermo spectrometer with a K-Alalpha source (ESCALAB 250Xi, USA). The contact angles (CA) of the resins were tested by the rotating drop interfacial tension meter (TX500 TM, USA). The pore structure parameters of the resins were tested by N$_2$ sorption at 77 K using the automatic surface area and porosity analyzer (Tristar 3000, USA), and values of S_{BET}, V_{total} and D_p were obtained from the N$_2$ isotherms. Values of pH were recorded on a pH meter (PHS-3C, China). Content of hydroxyl groups on the surface of PS-OH and HCPS-OH resins was measured by analyzing acid groups exchange capacity of resins. The concentration of MB, AN and PNA was recorded by the spectrophotometer (UV-2450, Japan) at 664 nm, 279 nm and 380 nm, respectively. Swelling ratio of the resins was determined by the ratio of the volume of the resins swollen in a given medium to the volume in the dry state.

2.4. Equilibrium and kinetic adsorption

25 mL MB aqueous solution (pH 4.8) with the initial concentrations of 100.0, 200.0, 300.0, 400.0, and 500.0 mg L^{-1} and 0.1 g resins were added in each glass stoppered conical flasks respectively. The isotherms at 298 K, 308 K, and 318 K were obtained by using a water-bathing constant temperature oscillator at 150 rpm. The equilibrium adsorption capacity of MB (q_e, mg g^{-1}) on resins was calculated according to the following formula,

$$q_e = (c_0 - c_e)/((1 - x)m) \tag{1}$$

where V (mL) is solution volume, c_0 and c_e (mg L^{-1}) are the MB concentration of initial and equilibrium, x (%) and m (mg) was the moisture holding capacity and mass of the wet resins, respectively.

For the kinetics adsorption, 250 mL of 500.5 mg L^{-1} MB aqueous solution (pH 4.8) and 1.0 g resins were added in a glass stoppered conical, and the flask was shaken with an oscillating rate of 150 rpm at 298 K. The supernatant was taken from the conical flask at specified time to test MB concentration.

2.5. Dynamic adsorption and regeneration

8.0 mL HCPS-OH-4 were densely packed in an adsorption column (16 mm of inner diameter). The MB solution
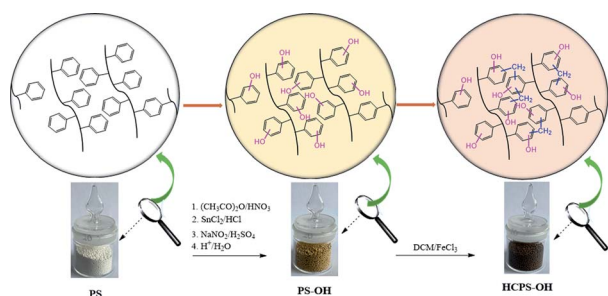
Scheme 1 Procedure for preparation of the HCPS-OH resins.

(482.0 mg L^{-1}) was passed down through the resin bed with a constant flow rate of 4 BV h^{-1} at room temperature (291.4 K). The effluents were collected, and the effluents with the concentration of 5% and 95% of the influent concentration were denoted as leakage-point and endpoint, respectively. After the equilibrium adsorption, the resin bed was regenerated by the following three steps: (i) rinsing with 1 BV de-ionized water (ii) rinsing with 20 BV 1.0 HCl methanol solution to remove MB on HCPS-OH-4 with a constant flow rate of 2 BV h^{-1}, (iii) washing with deionized water till the effluent was neutral. Thereafter, the regenerated resin bed was used in next four cycles of adsorption–regeneration.

3. Results and discussion

3.1. Structure of the resins

As displayed in Scheme 1, four PS-OH resins and four corresponding HCPS-OH resins were prepared with various content of hydroxyl groups by adjusting the extent of nitration of PS-co-DVB before reductive amination. The FT-IR spectra of PS-co-DVB, PS-NO$_2$, PS-NH$_2$ and PS-OH were shown in Fig. 1(a). It could be found that two new absorption band at 1522 cm^{-1} and 1344 cm^{-1} appeared in the spectrum of PS-NO$_2$ as compared with that of PS-co-DVB, which revealed that PS-co-DVB was nitrated successfully. After reductive amination, the N–H

stretching band at 3430 cm^{-1} strengthened observably while the N–O band at 1344 cm^{-1} disappeared, which implied that the nitro groups were reduced to amino groups successfully. Moreover, the content of amino groups in the PS-NH$_2$ resins was measured by analyzing the weak base exchange capacity via titration (Table S2†). In addition, the content of phenolic hydroxyl groups in the PS-OH resins was measured by analyzing the weak acid exchange capacity via titration (Table S3†), and the results confirmed that the amino groups in the PS-NH$_2$ resins were successfully converted to hydroxyl groups in the PS-OH resins.

The FT-IR spectra of the HCPS-OH resins were shown in Fig. 1(b). The stretching band of O–H at 3440 cm^{-1} and that of C–O at 1240 cm^{-1} appeared in all of the four spectra, and the intensity of the two absorption bands enhanced in the sequence from HCPS-OH-1 to HCPS-OH-4, which was in accordance with the results of hydroxyl groups content of the HCPS-OH resins (Table S4†). Furthermore, the analysis results of surface hydrophilicity by test of contact angles (CA) with water (Fig. S2†) demonstrated that the surface hydrophilicity of the HCPS-OH resins increased with the increase of hydroxyl groups content, implying the dispersion of hydroxyl groups in the pore surface of the HCPS-OH resins.

The elemental species of the HCPS-OH resins were determined by XPS and the results were shown in Fig. S3.† The O content increased from 3.51 wt% of HCPS-OH-1 to 14.34 wt% of HCPS-OH-4, demonstrating that about 2.5 mmol g^{-1} and 10.2 mmol g^{-1} hydroxyl groups were introduced in HCPS-OH-1 and HCPS-OH-4, respectively, which were much higher than the hydroxyl groups content determined by analyzing the weak acid exchange capacity (Table S4†) and implied most of the hydroxyl groups were dispersed in the pore surface of the HCPS-OH resins. In addition, the Cl specie of about 0.3 wt% presented in the HCPS-OH resins, which might be resulted from the Friedel–Crafts reaction between the PS-OH resins and DCM without further post-cross-linking. The N specie was almost disappeared in the HCPS-OH resins, demonstrating that nitro or amino groups in the intermediate resins were fully converted. Specifically, the high-resolution C1s spectrum in Fig. 2(a)
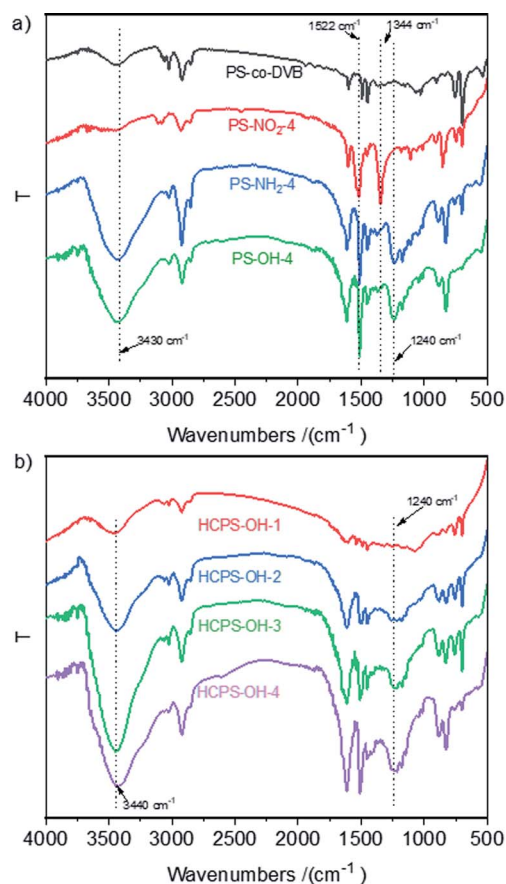

Fig. 1 FT-IR spectra of (a) PS-co-DVB, PSNO$_2$-4, PS-NH$_2$-4 and PS-OH-4, (b) the HCPS-OH resins.
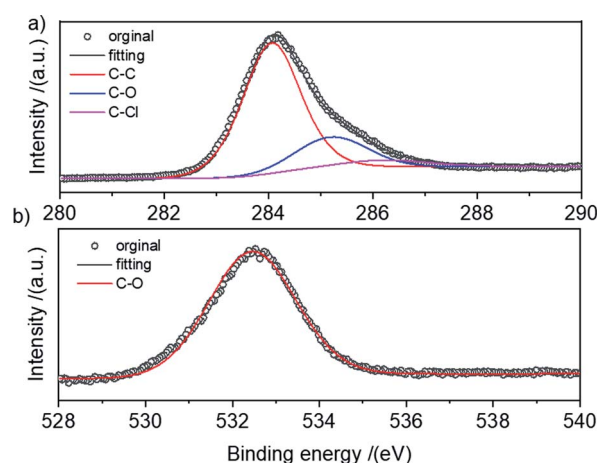

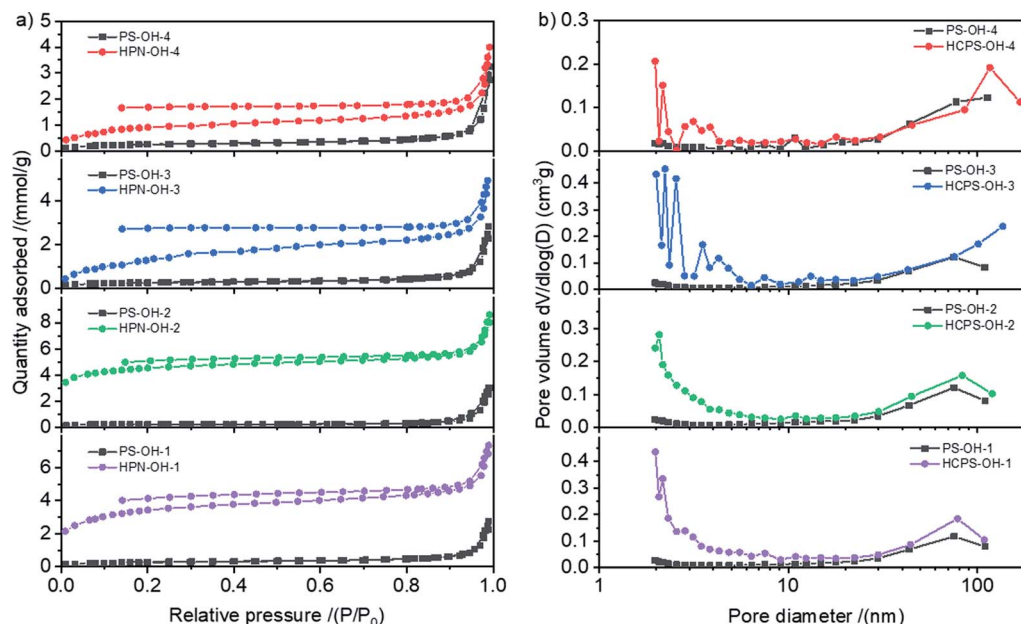Fig. 2 XPS spectra of (a) C1s and (b) O1s of HCPS-OH-4.

Fig. 3 (a) N_2 sorption isotherms for the PS–OH and HCPS–OH resins at 77 K, and (b) the corresponding PSD curves.

displayed that the C–O and C–Cl configurations presented with the binding energy at 285.2 eV and 286.2 eV, respectively. The high-resolution O1s spectrum in Fig. 2(b) at 532.4 eV suggested that O presented only in the form of C–OH configuration for HCPS-OH-4.

The N_2 sorption isotherms of the PS–OH and HCPS–OH resins were displayed in Fig. 3(a). The HCPS–OH resins had much greater N_2 adsorption capacities than the corresponding PS–OH resins. The pore size distribution (PSD) curves obtained from the N_2 sorption isotherms were displayed in Fig. 3(b), and the results showed that the HCPS–OH resins had hierarchic porosity with abundant micro/mesopores (pore diameter less than 10 nm) and significant meso/macropores (pore diameter more than 10 nm), but the PS–OH resins had hardly micro/ mesopores, which indicated that the post-cross-linking reaction resulted in the abundant micro/mesopores in the HCPS-OH resins.

Pore structure parameters of the resins were shown in Table 1. It could be seen from Table 1 that S_{BET} of the HCPS-OH resins

were all much higher than that of the corresponding PS–OH resins. There were not significant differences between the pore structure of the four PS–OH resins, but the S_{BET} of the HCPS–OH resins were quite different, which might be resulted from the difference of swelling ratio in DCM and reactivity in post-cross-linking between the four PS–OH resins. As shown in Fig. S4,† the swelling ratio of the PS–OH resins in DCM decreased with the increase of hydroxyl groups content of the resins, and thus more micro/mesopores was formed in the less hydroxylated resins by post-cross-linking in the swollen state, and resulted in the higher S_{BET}. In the other hand, reactivity of the hydroxylated benzene rings in the electrophilic post-cross-linking reaction was higher than that of the un-hydroxylated benzene rings, which made the S_{BET} of HCPS-OH-2 (315.1 m^2 g^{-1}) be higher than that of HCPS-OH-1 (247.0 m^2 g^{-1}). The swelling ratio of the HCPS–OH resins in water and some organic solvents (*i.e.* ethanol, acetone, and DCM) were shown in Fig. S5.† The results indicated that swelling ratio of the HCPS-OH resins in oxygen-containing solvents (*i.e.* water, ethanol,

Table 1 Structure parameters of the resins

Code	S_{BET} (m^2 g^{-1})	S_{micro} (m^2 g^{-1})	V_{total} (cm^3 g^{-1})	V_{micro} (cm^3 g^{-1})	D_P (nm)	Q_{OH}^a (mmol g^{-1})	MHC (%)
PS-*co*-DVB	19.5	—	0.039	—	24.28	—	—
PS-OH-1	20.5	—	0.044	—	24.63	1.2	46.4
PS-OH-2	20.4	1.2	0.043	0.001	25.12	2.3	49.9
PS-OH-3	20.5	1.7	0.043	0.001	28.54	3.9	52.7
PS-OH-4	20.9	1.6	0.042	0.001	30.31	5.4	57.4
HCPS-OH-1	247.0	56.4	0.192	0.035	6.89	1.4	52.6
HCPS-OH-2	315.1	175.4	0.226	0.096	8.61	2.2	53.9
HCPS-OH-3	118.5	34.6	0.114	0.023	6.02	3.7	54.2
HCPS-OH-4	69.0	5.3	0.078	0.011	11.71	5.0	57.8

^{a} Q_{OH} = quantity of hydroxyl groups determined by weak acid exchange capacity analysis.

and acetone) increased with the increase of hydroxyl groups content of the resins, whereas the swelling ratio in DCM was bigger for the less hydroxylated resins, which might be resulted from the hydrogen bonding between the hydroxyl groups of the resins and oxygen atoms of the solvent. The bigger swelling ratio for the more hydroxylated resins in water implied the higher S_{BET} in water than that tested by N_2 adsorption–desorption in dry state. Moisture holding capacity (MHC) of the HCPS-OH resins were higher than that of the corresponding PS-OH resins, which was in accordance with the generation of micro/mesopores in post-cross-linking.

3.2. Equilibrium adsorption and thermodynamics

The equilibrium isotherms of MB on the PS-OH resins and corresponding HCPS-OH resins from water at 298 K were displayed in Fig. 4. All of the four HCPS-OH resins possessed a higher equilibrium capacity as compared with the corresponding PS-OH resins, which should be attributed to the enhanced S_{BET} and V_{total}. According to fitting equation, the equilibrium capacity ranked the order of HCPS-OH-4 (203.6 mg g^{-1}) > HCPS-OH-2 (135.2 mg g^{-1}) > HCPS-OH-3 (132.4 mg g^{-1}) > HCPS-OH-1 (51.2 mg g^{-1}) at the equilibrium concentration of

20 mg L^{-1}. HCPS-OH-4 had much less S_{BET} as compared with the other HCPS-OH resins, but it possessed much bigger adsorption capacity, indicating that the hydroxyl groups acted as important role in the adsorption. Fig. S6† presented the equilibrium adsorption isotherms of MB on the HCPS-OH resins at 298 K, 308 K, and 318 K, respectively. The equilibrium data were fitted by Langmuir, Freundlich and Redlich–Peterson isotherm equations,[43,44] and the corresponding fitting parameters were displayed in Table 2.

The results showed the Redlich–Peterson isotherm equation fitted better than the Langmuir and Freundlich equations. The correlation coefficient R^2 and the empirical constant α indicated that the equilibrium adsorption of MB on the PS-OH resins and HCPS-OH-4 were mainly based on monolayer adsorption, while adsorption on HCPS-OH-1, HCPS-OH-2 and HCPS-OH-3 were mainly based on multiple-layers adsorption.

According to the Van't Hoff equation, ΔH and ΔS can be obtained by the slopes and intercepts of the fitting straight $\ln K_c$ versus $1/T$ (in Fig. S7†), and the thermodynamic parameters were displayed in Table S5.† The ΔH was positive, confirming the endothermic process for MB adsorption. Meanwhile, the negative ΔG and positive ΔS implied a spontaneous and disordered adsorption process at 298 K, 308 K, and 318 K.
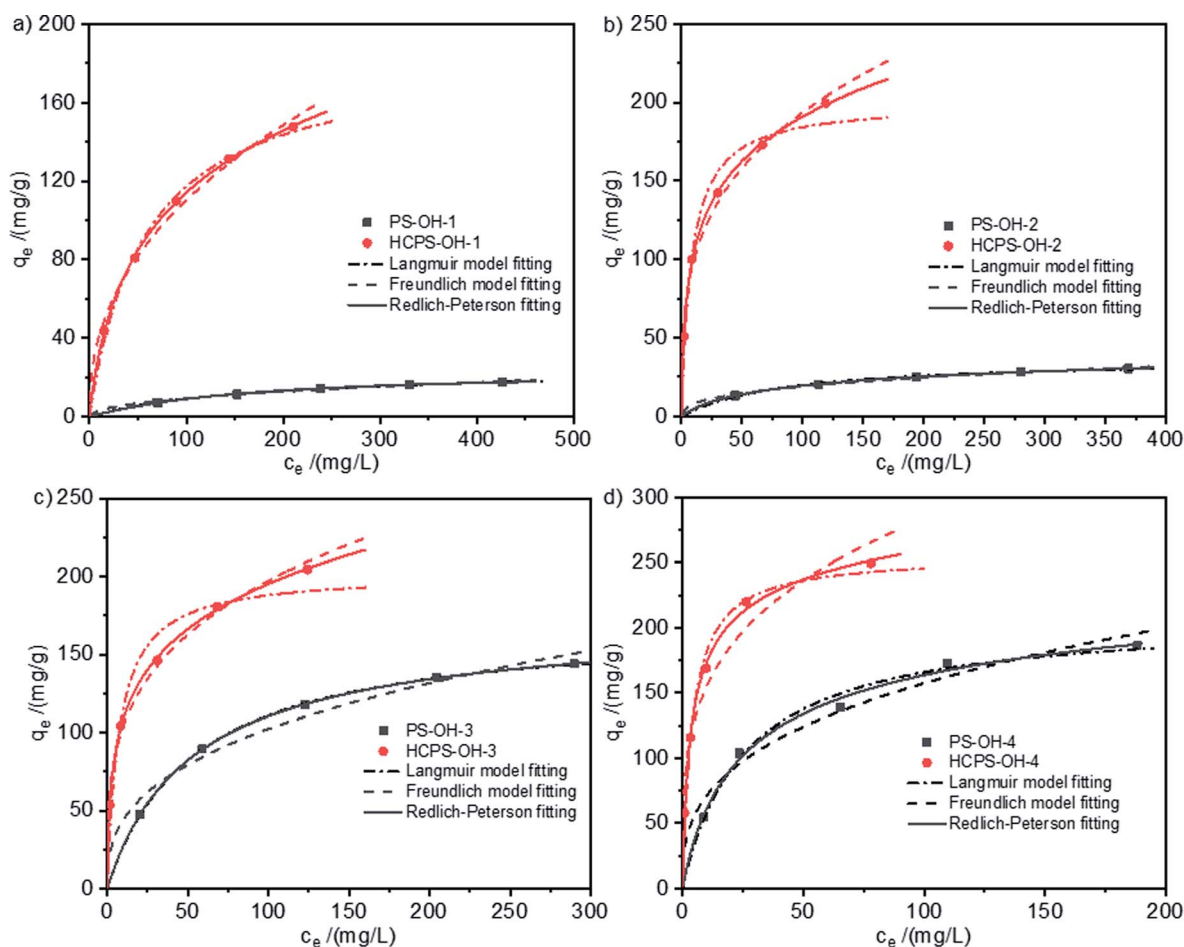

Fig. 4 Equilibrium isotherms of MB on (a) PS-OH-1 and HCPS-OH-1, (b) PS-OH-2 and HCPS-OH-2, (c) PS-OH-3 and HCPS-OH-3, and (d) PS-OH-4 and HCPS-OH-4 at 298 K.

Table 2 Adsorption isotherm model parameters for the adsorption of MB on resins

Code	T (K)	Langmuir model			Freundlich model			Redlich–Peterson model			
		q_m (mg g^{-1})	$K_L/10^{-3}$ (L mg^{-1})	R^2	K_F [(mg g^{-1}) (L mg^{-1})$^{1/n}$]	$1/n$	R^2	q_{mon} (mg g^{-1})	b_{RP} (L mg^{-1})	α	R^2
PS-OH-1	298	24.6	5.58	0.997	1.01	0.473	0.967	53.1	0.006	1	0.997
PS-OH-2	298	37.0	11.29	0.993	3.27	0.380	0.985	13.4	0.045	0.837	0.999
PS-OH-3	298	170.1	18.76	0.999	19.13	0.364	0.950	150.2	0.022	0.979	0.999
PS-OH-4	298	208.9	38.58	0.982	32.31	0.344	0.946	122.9	0.830	0.900	0.982
	298	185.6	17.15	0.982	15.09	0.432	0.985	58.8	0.083	0.798	0.999
HCPS-OH-1	308	205.7	18.56	0.975	17.11	0.431	0.993	32.4	0.338	0.673	0.995
	318	212.8	23.87	0.948	21.67	0.411	0.996	24.7	2.584	0.612	0.994
	298	200.0	117.78	0.947	50.40	0.292	0.981	78.4	0.799	0.780	0.999
HCPS-OH-2	308	207.3	157.82	0.926	57.53	0.286	0.988	77.6	1.572	0.780	0.999
	318	209.7	209.69	0.923	64.19	0.275	0.990	84.8	1.981	0.789	0.999
	298	202.1	134.68	0.924	55.15	0.277	0.986	75.4	1.315	0.789	0.999
HCPS-OH-3	308	211.0	165.45	0.899	61.60	0.274	0.993	74.6	2.870	0.769	0.999
	318	215.4	220.12	0.881	70.21	0.259	0.994	80.9	4.988	0.774	0.999
	298	255.5	245.77	0.982	84.91	0.262	0.918	172.4	0.529	0.905	0.995
HCPS-OH-4	308	250.1	318.99	0.973	89.36	0.252	0.926	163.4	0.758	0.893	0.996
	318	241.3	477.23	0.949	96.12	0.236	0.939	150.0	1.401	0.875	0.994

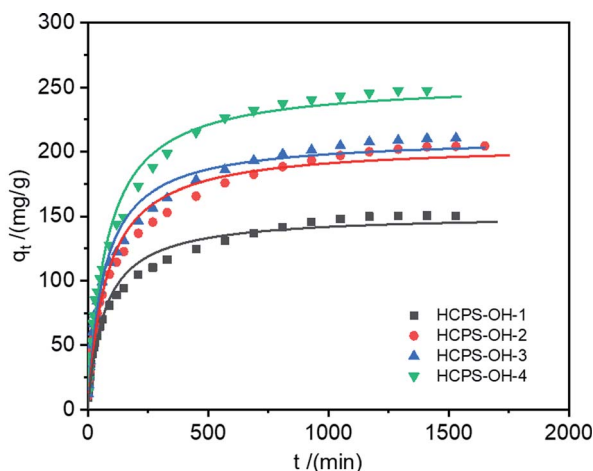**Fig. 5** The adsorption kinetic curves of MB on the HCPS-OH resins at 298 K.

3.3. Adsorption kinetics

The adsorption kinetics is also an important index that evaluates the removal efficiency and feasibility of MB by the HCPS-OH resins. Fig. 5 displayed the adsorption kinetic curves of MB (c_0: 500.5 mg L^{-1}) on the HCPS-OH resins (beads diameter: 0.7 mm) at 298 K, and Fig. S8† displayed the adsorption kinetic curves of MB on HCPS-OH-4 at various temperature. The pseudo-first-order and pseudo-second-order rate equations were used to fit the kinetic data, and the relevant parameters were listed in Table 3. The pseudo-second-order rate equation was more suitable to describe the kinetic behavior, and the interaction between the –OH groups and MB affected the MB diffusion into HCPS-OH-4. Specifically, higher temperature would shorten the time to the adsorption equilibrium. Furthermore, the intra-particle diffusion model was adopted to explain the kinetic behavior in Fig. S9.† The fitted lines showed good linearity originally and passed through the original point, indicating that the intra-particle diffusion was the rate-limiting step.

3.4 Effect of inorganic salts on MB adsorption

Existence of inorganic salts in the MB solution could increase the ionic strength and lower the solubility of MB. Fig. S10† displayed the equilibrium adsorption capacity of MB on the

Table 3 Correlated parameters for the kinetic data of MB adsorption on HCPS-OH by pseudo-first-order and pseudo-second-order equations fitting

Code	T (K)	Pseudo-first-order			Pseudo-second-order		
		q_e (mg g^{-1})	$k_1/10^{-3}$ (min^{-1})	R^2	q_e (mg g^{-1})	$k_2/10^{-5}$ (g (mg min)$^{-1}$)	R^2
HCPS-OH-1	298	137.8	10.80	0.937	151.6	9.50	0.981
HCPS-OH-2	298	187.4	9.38	0.939	206.1	6.15	0.982
HCPS-OH-3	298	192.5	11.07	0.938	211.3	7.05	0.983
	298	230.3	9.74	0.950	254.9	5.12	0.985
HCPS-OH-4	308	230.3	14.15	0.926	251.8	7.70	0.977
	318	230.5	19.56	0.899	251.9	10.67	0.966
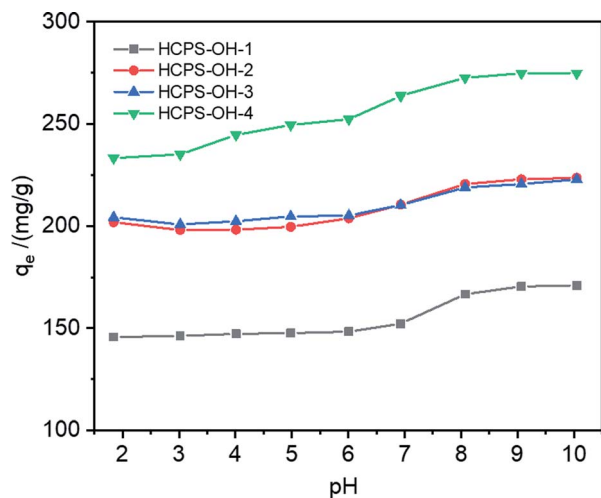
Fig. 6 Equilibrium adsorption capacity of MB on the HCPS-OH resins from aqueous solution of various pH.

Fig. 8 Equilibrium concentration of MB and removal efficiency by adsorption with various concentration of HCPS-OH-4.

HCPS-OH resins from the MB solutions with various concentration of KCl.

An increase in ionic strength resulted in the increased MB removal capacity of HCPS-OH, which may be resulted from the salting-out effect of MB by adding electrolytes. The reduction of MB solubility would bring out the enhancement of hydrophobic interaction between the adsorbents and MB. The results showed that adsorption capacity on the HCPS-OH resins increased with the increase of KCl concentration, which indicated that the co-existence of inorganic salts would benefit the adsorptive removal of MB from aqueous solution.

3.5. Effect of pH on MB adsorption

The pH of MB solution could influence the existence form of phenolic hydroxyl groups as well as the swelling ratio of the HCPS-OH resins, and thus could affect the adsorption capacity of MB. Fig. 6 displayed the equilibrium adsorption capacity of MB on the HCPS-OH resins from aqueous solution of various pH. The results showed that adsorption capacity on the HCPS-OH resins increased with the increase of pH. At the lower pH, the phenolic hydroxyl groups of the HCPS-OH resins were hydrogen bonding donors and could form hydrogen bonds with the nitrogen atoms of MB, and the aromatic matrix of the resins
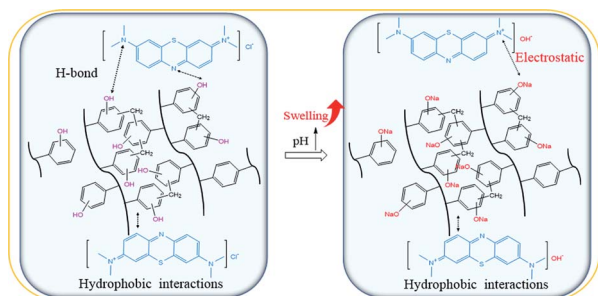
interacted with the planar MB molecules *via* hydrophobic interactions, and thus MB was adsorbed on the resins. Hydrophobic and hydrogen bonding interactions should be the dominant driving force for MB adsorption at the lower pH. With the increase of pH by adjusting the initial MB solution with NaOH, the phenolic hydroxyl groups of the resins deprotonated to $-O^-Na^+$ gradually, which could interact with MB through electrostatic interaction instead of hydrogen bonding (in Fig. 7), and thus the adsorption capacity increased with the pH increasing due to the stronger interaction of electrostatic interaction as compared with hydrogen bonding. In addition, the $-O^-Na^+$ groups were more hydrophic than the hydroxyl groups, and thus the HCPS-OH resins swelled to higher extent in solutions of higher pH (in Fig. S11†), which resulted in higher accessability of functional groups and higher adsorption capacity.

3.6. Effect of the resin concentration on MB adsorption

Effect of the resin dosage on adsorptive removal of MB from water was investigated by adsorption of MB with various concentration of HCPS-OH-4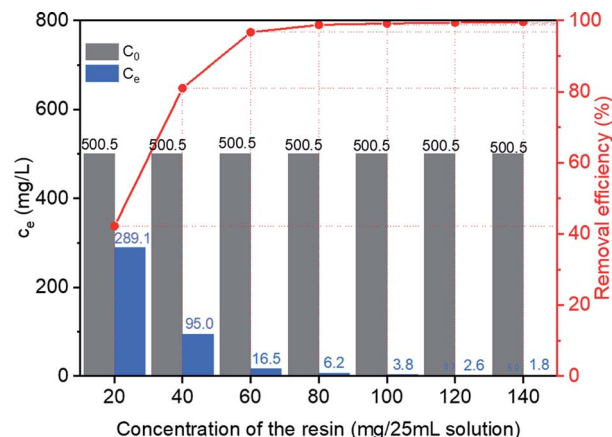. Equilibrium concentration of MB and removal efficiency by adsorption with various concentration of HCPS-OH-4 were presented in Fig. 8. The results showed that the removal efficiency increased rapidly to 99.2% at the resin dosage of 100 mg/25 mL, then increased to 99.6% at the resin dosage of 140 mg/25 mL, and the residue concentration of MB decreased to 1.8 mg L^{-1}, which satisfied the tertiary grade wastewater discharge standard (<2 mg L^{-1}) for printing and dyeing wastewater by Chinese environmental protection authorities, demonstrating that HCPS-OH-4 is an efficient polymeric adsorbent for treatment of MB wastewater.

3.7. Adsorption selectivity

The adsorption isotherms of MB on the HCPS-OH resins from aqueous solutions of MB and its mixture with AN or PNA were shown in Fig. 9, and the adsorption isotherms for AN and PNA were shown in Fig. S12.† In Fig. 9(a) and (b), the adsorption capacity of MB on HCPS-OH-1 and HCPS-OH-2 from the mixture
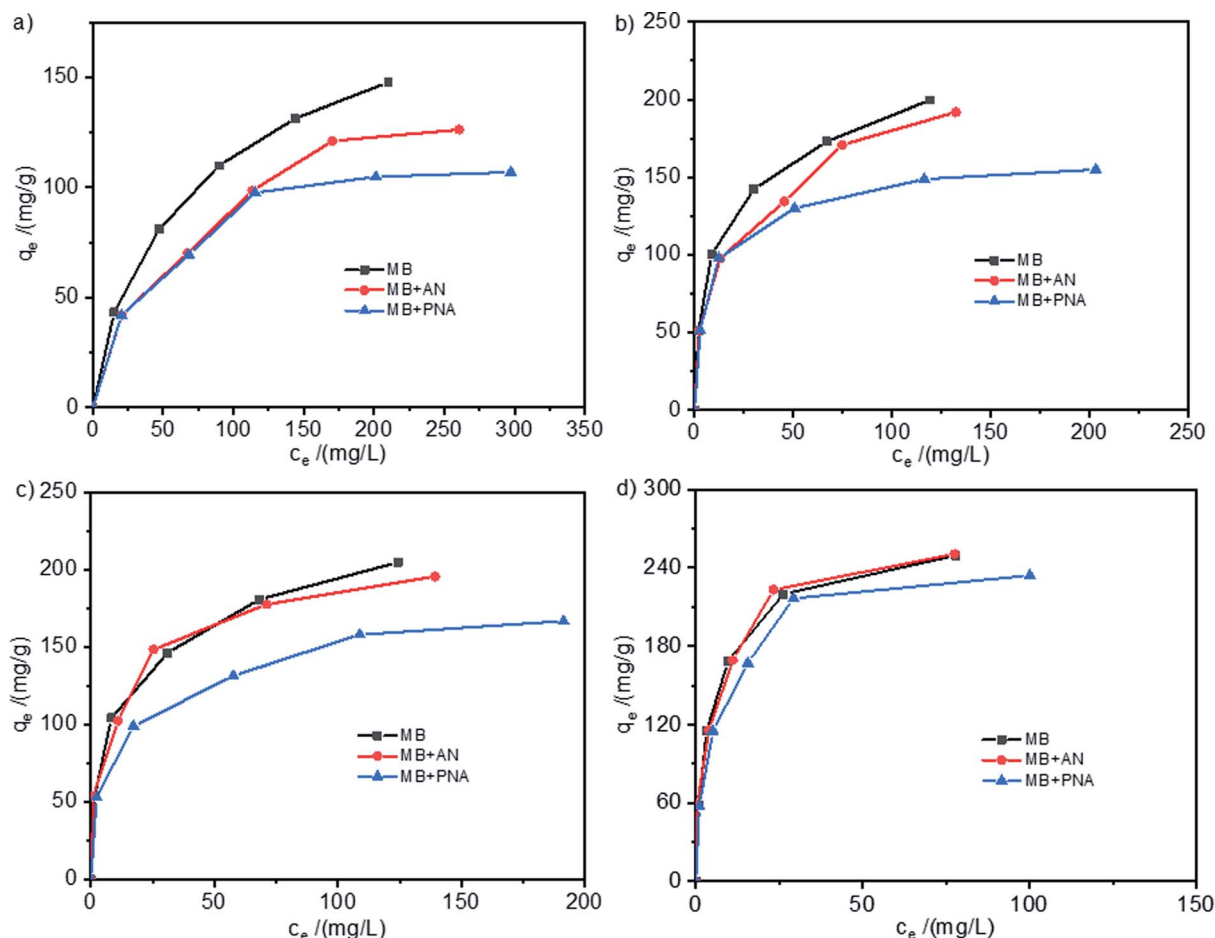

Fig. 7 Possible adsorption mechanism of MB on the HCPS-OH resins.

Fig. 9 Adsorption isotherms of MB on (a) HCPS-OH-1, (b) HCPS-OH-2, (c) HCPS-OH-3 and (d) HCPS-OH-4 from solutions of MB, MB + AN, and MB + PNA.

solution of MB + AN or MB + PNA at higher concentration was apparently lower than that from the single-component solution of MB, which might be resulted from the competitive adsorption of AN and PNA due to micropore/mesopore filling. In addition, the adsorption capacity of MB was almost same at lower concentrations due to more adsorption sites. However, most of the adsorption sites were occupied at higher MB concentration, and the stronger competitive adsorption of PNA caused a greater negative impact on adsorption of MB. It can be seen from Fig. 9(c) and (d) that the adsorption capacity of MB on HCPS-OH-3 and HCPS-OH-4 from the MB + AN solution was almost the same with that from the single-component solution of MB, while that from the MB + PNA was relatively lower. The possible reason is that the pores of HCPS-OH-3 and HCPS-OH-4 were mainly composed of meso/macropores, and thus the competitive adsorption of AN resulted from micropore/mesopore filling could be ignored. However, PNA might interact with the HCPS-OH resins through hydrogen bonding between the nitro groups of PNA and hydroxyl groups of the resins, which resulted in less hydroxyl groups interacting with MB and lowered the adsorption capacity.

3.8. Dynamic adsorption and recyclability

The dynamic adsorption and desorption of MB on HCPS-OH-4 was performed, and the results were shown in Fig. 10. The corresponding breakthrough point (at $c/c_0 = 0.05$) and saturated point (at $c/c_0 = 0.95$) were measured to be 110–115 BV and 330–335 BV, respectively. The dynamic adsorption capacity of MB was calculated to be 100.9 g L^{-1} (293.9 mg g^{-1}). The adsorption of MB on HCPS-OH-4 was mainly based on hydrogen-bond and hydrophobic interactions. 1.0 M HCl methanol solution was used as desorption solvent since HCl could break the hydrogen bond through combination with the nitrogen atoms of MB and methanol could dispel the hydrophobic interactions between HCPS-OH-4 and MB. Therefore, the resin bed was washed with 20 BV of 1.0 M HCl methanol solution to desorb MB from HCPS-OH-4, and about 92.2% of the MB was desorbed. The continuous adsorption–regeneration cycles were accomplished for 5 times and the results were displayed in Fig. 10(c). The adsorption capacity amounted to 245.4 mg g^{-1} even after 5 cycles, exhibiting outstanding recyclability.

As compared with some other adsorbing materials for adsorptive removal of MB, HCPS-OH-4 showed higher adsorption capacity (203.6 mg g^{-1}) than many materials at the MB
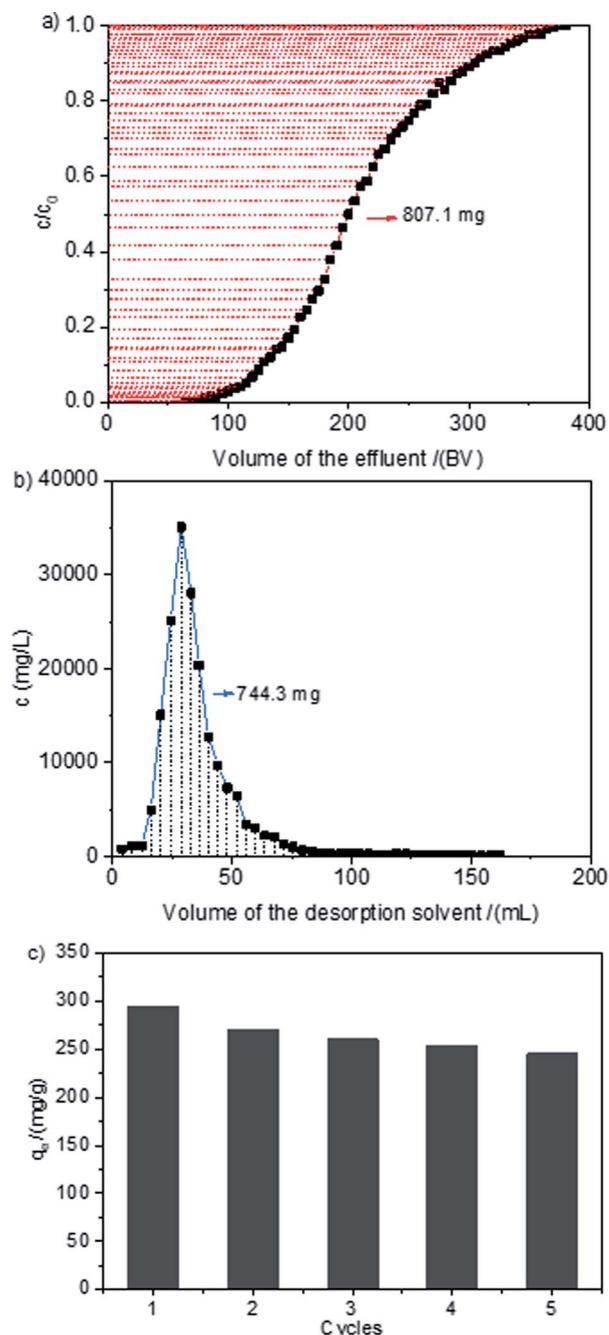
Fig. 10 Dynamic (a) adsorption and (b) desorption curves of MB on HCPS-OH-4, and (c) adsorption capacities of MB on HCPS-OH-4 for five adsorption–regeneration.

concentration of 20 mg L^{-1}, such as silica-based adsorbents (Ce-HECMS of 169.2 mg g^{-1}, Ti-SBA-15 of 154.9 mg g^{-1}), paper materials (T-AC of 24.0 mg g^{-1}), commercial activated carbon (Merck of 145.9 mg g^{-1}), straw materials (CSHUPC of 166.0 mg g^{-1}), modified hectorite (MSH-AB-W of 179.6 mg g^{-1}), tree bark (GTB of 130.2 mg g^{-1}, FCBAC of 21.2 mg g^{-1}), kaolin (KT3B of 69.0 mg g^{-1}) and modified lignin and alginate hybrid spherical adsorbents (Alg/C-Lig of 141.3 mg g^{-1}). However, HCPS-OH-4 had a less equilibrium capacity than coconut shell-based

Table 4 Comparison of the equilibrium capacity (q_e) of MB on HCPS-OH-4 with some other adsorbents in the literature at 20 mg L^{-1}

Adsorbents	q_e (mg g^{-1})	Ref.
Ce-HECMS	169.2	13
Ti-SBA-15	154.9	45
T-AC	24.0	46
Merck	145.9	47
CSHUPC	166.0	21
MSH-AB-W	179.6	14
GTB	130.2	17
FCBAC	21.2	48
KT3B	69.0	15
Alg/C-Lig	141.3	49
AC-3	891.5	50
Waste paper-based activated carbon	1432.1	20
HCPS-OH-4	203.6	This study

activated carbon (AC-3 of 891.5 mg g^{-1}) and waste paper-based activated carbon (1432.1 mg g^{-1}) (Table 4).

4. Conclusion

Phenolic hydroxyl groups were introduced in the PS resin to obtain a series of PS-OH resins with various content of hydroxyl groups, and then the PS-OH resins were post-crosslinked by the double Friedel–Crafts reaction with DCM to obtain the corresponding HCPS-OH resins. The HCPS-OH resins had phenolic hydroxyl groups uploading of 1.4–5.0 mmol g^{-1} and S_{BET} of 69.0–315.1 $m^2 g^{-1}$, and showed effective adsorption for MB. The adsorption capacity of MB on HCPS-OH-4 amounted to 293.9 mg g^{-1} for MB solution with a concentration of 482.0 mg L^{-1}, indicating that its adsorption performance was better than many other adsorbing materials reported in the literature. Hydrogen bonding and hydrophobic interactions might be the main driving forces for adsorption of MB. Factors such as higher temperature, higher pH and co-existing ions had a positive effect on the adsorption, and the removal efficiency of MB reached 99.6% as the HCPS-OH-4 dose increased to 140 mg/ 25 mL. In particular, the adsorbent HCPS-OH-4 showed adsorption selectivity for MB in the MB + AN and MB + PNA mixture solutions. Moreover, the adsorbent HCPS-OH-4 in this paper had an outstanding recyclability, and it could be rapidly regenerated using 1.0 M HCl methanol solution.

Author contributions

Fada Li: conceptualization, methodology, formal analysis, writing-original draft. Jun Liu: validation, visualization. Wenxiu Liu: investigation. Yuanyuan Xu: investigation. Yiwen Cao: investigation. Bo Chen: supervision. Mancai Xu: resources, writing-review & editing.

Conflicts of interest

There are no conflicts to declare.

References

1 Q. Li, Y. Li, X. Ma, Q. Du, K. Sui, D. Wang, C. Wang, H. Li and Y. Xia, *Chem. Eng. J.*, 2017, **316**, 623–630.

2 J. He, A. Cui, S. Deng and J. P. Chen, *J. Colloid Interface Sci.*, 2018, **512**, 190–197.

3 N. My Tran, Q. Thanh Hoai Ta, A. Sreedhar and J.-S. Noh, *Appl. Surf. Sci.*, 2021, **537**, 148006.

4 S.-A. Ong, L.-N. Ho and Y.-S. Wong, *Desalin. Water Treat.*, 2015, **54**, 557–561.

5 S. Govindwar, A. Bedekar, S. Kshirsagar and A. Gholave, *RSC Adv.*, 2015, **5**, 99228–99239.

6 S. R. Geed, K. Samal and A. Tagade, *J. Environ. Chem. Eng.*, 2019, **7**, 103439.

7 T. Zhang, J. Xu, J. Qian and J. Zhang, *J. Mater. Sci.*, 2020, **55**, 13605–13617.

8 X. Liu, Y. Yang, X. Shi and K. Li, *J. Hazard. Mater.*, 2015, **283**, 267–275.

9 A. M. Cahino, R. G. Loureiro, J. Dantas, V. S. Madeira and P. C. Ribeiro Fernandes, *Ceram. Int.*, 2019, **45**, 13628–13636.

10 S. Yu, X. Wang, H. Pang, R. Zhang, W. Song, D. Fu, T. Hayat and X. Wang, *Chem. Eng. J.*, 2018, **333**, 343–360.

11 G. Fadillah, T. A. Saleh, S. Wahyuningsih, E. Ninda Karlina Putri and S. Febrianastuti, *Chem. Eng. J.*, 2019, **378**, 122140.

12 M. Soniya and G. Muthuraman, *J. Ind. Eng. Chem.*, 2015, **30**, 266–273.

13 R. Lyu, C. Zhang, T. Xia, S. Chen, Z. Wang, X. Luo, L. Wang, Y. Wang, J. Yu and C. Wang, *Colloids Surf., A*, 2020, **606**, 125425.

14 R. R. Pawar, L. Lalhmunsiama, P. Gupta, S. Y. Sawant, B. Shahmoradi and S.-M. Lee, *Int. J. Biol. Macromol.*, 2018, **114**, 1315–1324.

15 L. Mouni, L. Belkhiri, J.-C. Bollinger, A. Bouzaza, A. Assadi, A. Tirri, F. Dahmoune, K. Madani and H. Remini, *Appl. Clay Sci.*, 2018, **153**, 38–45.

16 L. Chen, Y. Li, Q. Du, Z. Wang, Y. Xia, E. Yedinak, J. Lou and L. Ci, *Carbohydr. Polym.*, 2017, **155**, 345–353.

17 P. T. Hernandes, M. L. S. Oliveira, J. Georgin, D. S. P. Franco, D. Allasia and G. L. Dotto, *Environ. Sci. Pollut. Res.*, 2019, **26**, 31924–31933.

18 L. Sellaoui, D. Franco, H. Ghalla, J. Georgin, M. S. Netto, G. Luiz Dotto, A. Bonilla-Petriciolet, H. Belmabrouk and A. Bajahzar, *Chem. Eng. J.*, 2020, **394**, 125011.

19 Z. Li, H. Hanafy, L. Zhang, L. Sellaoui, M. Schadeck Netto, M. L. S. Oliveira, M. K. Seliem, G. Luiz Dotto, A. Bonilla-Petriciolet and Q. Li, *Chem. Eng. J.*, 2020, **388**, 124263.

20 X. Tang, G. Ran, J. Li, Z. Zhang and C. Xiang, *J. Hazard. Mater.*, 2021, **402**, 123579.

21 X. Xing, W. Jiang, S. Li, X. Zhang and W. Wang, *Waste Manage.*, 2019, **89**, 64–72.

22 C. Urita, K. Urita, T. Araki, K. Horio, M. Yoshida and I. Moriguchi, *J. Colloid Interface Sci.*, 2019, **552**, 412–417.

23 G. Jiangfei, W. Lizhi, D. Zhang and J. Huang, *Energy Fuels*, 2020, **34**, 9771–9778.

24 L. Wang, Q. Xiao, D. Zhang, W. Kuang, J. Huang and Y.-N. Liu, *ACS Appl. Mater. Interfaces*, 2020, **12**, 36652–36659.

25 S. N. Lanin, S. A. Platonova, A. E. Vinogradov, K. S. Lanina, E. P. Nesterenko and P. N. Nesterenko, *Adsorption*, 2020, **26**, 339–348.

26 G. H. Gunasekar and S. Yoon, *J. Mater. Chem. A*, 2019, **7**, 14019–14026.

27 G. Liu, Y. Wang, C. Shen, Z. Ju and D. Yuan, *J. Mater. Chem. A*, 2015, **3**, 3051–3058.

28 R. Castaldo, V. Ambrogi, R. Avolio, M. Cocca, G. Gentile, M. Emanuela Errico and M. Avella, *Chem. Eng. J.*, 2019, **362**, 497–503.

29 J. Zhang, Z.-A. Qiao, S. M. Mahurin, X. Jiang, S.-H. Chai, H. Lu, K. Nelson and S. Dai, *Angew. Chem., Int. Ed.*, 2015, **54**, 4582–4586.

30 N. Wang, C. Shen, T. Wang, Z. Liu, J. Dai and Z. Fei, *J. Taiwan Inst. Chem. Eng.*, 2019, **102**, 403–414.

31 M. Ghafari, Y. Cui, A. Alali and J. D. Atkinson, *J. Hazard. Mater.*, 2019, **361**, 162–168.

32 W. Kuang, Y.-N. Liu and J. Huang, *J. Colloid Interface Sci.*, 2017, **487**, 31–37.

33 Y. Gan, G. Chen, Y. Sang, F. Zhou, R. Man and J. Huang, *Chem. Eng. J.*, 2019, **368**, 29–36.

34 X. Wang, H. Li and J. Huang, *J. Colloid Interface Sci.*, 2017, **505**, 585–592.

35 A. Li, Q. Zhang, J. Chen, Z. Fei, C. Long and W. Li, *React. Funct. Polym.*, 2001, **49**, 225–233.

36 Z. Fu, H. Li, L. Yang, H. Yuan, Z. Jiao, L. Chen, J. Huang and Y.-N. Liu, *Chem. Eng. J.*, 2015, **273**, 240–246.

37 X. Jiang and J. Huang, *J. Colloid Interface Sci.*, 2016, **467**, 230–238.

38 Z. Fu and J. Huang, *Fluid Phase Equilib.*, 2017, **438**, 1–9.

39 L. Shao and J. Huang, *J. Colloid Interface Sci.*, 2017, **507**, 42–50.

40 J. Huang, H. Zha, X. Jin and S. Deng, *Chem. Eng. J.*, 2012, **195–196**, 40–48.

41 Y. Wang, Y. Gan and J. Huang, *Ind. Eng. Chem. Res.*, 2020, **59**, 11275–11283.

42 S. Pramanik, S. Dey and P. Chattopadhyay, *Anal. Chim. Acta*, 2007, **584**, 469–476.

43 I. Langmuir, *J. Am. Chem. Soc.*, 1916, **38**, 2221–2295.

44 H. M. F. Freundlich, *Z. Phys. Chem.*, 1906, **57**, 385–470.

45 T. Qiang, Y. Song, J. Zhao and J. Li, *J. Alloys Compd.*, 2019, **770**, 792–802.

46 A. Durairaj, T. Sakthivel, S. Ramanathan, A. Obadiah and S. Vasanthkumar, *Cellulose*, 2019, **26**, 3313–3324.

47 B. Bestani, N. Benderdouche, B. Benstaali, M. Belhakem and A. Addou, *Bioresour. Technol.*, 2008, **99**, 8441–8444.

48 D. Pathania, S. Sharma and P. Singh, *Arabian J. Chem.*, 2017, **10**, S1445–S1451.

49 J.-C. Kim, J. Kim, J. Park, J.-K. Oh, I.-G. Choi and H. W. Kwak, *React. Funct. Polym.*, 2021, **161**, 104839.

50 A. L. Cazetta, A. M. M. Vargas, E. M. Nogami, M. H. Kunita, M. R. Guilherme, A. C. Martins, T. L. Silva, J. C. G. Moraes and V. C. Almeida, *Chem. Eng. J.*, 2011, **174**, 117–125.